JOURNAL OF SOLID STATE CHEMISTRY **138,** 321–328 (1998)
ARTICLE NO. SC987791

Group 10 and Group 12 One-Dimensional Selenodiphosphates: $A_2MP_2Se_6$ (A = K, Rb, Cs; M = Pd, Zn, Cd, Hg)

Konstantinos Chondroudis and Mercouri G. Kanatzidis[1]

Department of Chemistry, Michigan State University, East Lansing, Michigan 48824

Received September 29, 1997; in revised form February 9, 1998; accepted February 17, 1998

The reaction of M (M = Pd, Zn, Cd, Hg) with a molten mixture of $A_2Se/P_2Se_5/Se$ produced the quaternary compounds $A_2MP_2Se_6$ (A = K, Rb, Cs; M = Pd, Zn, Cd, Hg). The crystals of $A_2MP_2Se_6$ are air- and water-stable. For $Cs_2PdP_2Se_6$ (1): monoclinic $C2/c$ (No. 15) with $a = 12.9750(4)$ Å, $b = 8.3282(2)$ Å, $c = 13.0568(1)$ Å, $\beta = 102.940(2)^\circ$, $Z = 4$, and $R/R_w = 6.7/7.5\%$. $K_2ZnP_2Se_6$ (2), $K_2CdP_2Se_6$ (3), $Rb_2CdP_2Se_6$ (4), and $Cs_2CdP_2Se_6$ (5) are isostructural. $Rb_2CdP_2Se_6$ (4): monoclinic $P2_1/n$ (No. 14) with $a = 6.640(1)$ Å, $b = 12.729(2)$ Å, $c = 7.778(1)$ Å, $\beta = 98.24(1)^\circ$, $Z = 2$, and $R/R_w = 3.7/4.9\%$. $K_2HgP_2Se_6$ (6) and $Rb_2HgP_2Se_6$ (7), are isostructural. $K_2HgP_2Se_6$ (6): monoclinic $P2_1/c$ (No. 14) with $a = 13.031(2)$ Å, $b = 7.308(2)$ Å, $c = 14.167(2)$ Å, $\beta = 110.63(1)^\circ$, $Z = 4$, and $R/R_w = 5.6/7.1\%$. Compounds 1–7 contain the ethane-like $[P_2Se_6]^{4-}$ group. Compound 1 has a one-dimensional structure with Pd^{2+} in square-planar coordination. Compounds 2–5 also have one-dimensional structures related to the TiI_3 structure type. The M^{2+} ions and the P–P pairs reside in Se octahedra that share opposite faces in the chain direction. Compounds 6 and 7 have a related one-dimensional structure but with Hg^{2+} in tetrahedral coordination. The solid state single-crystal optical absorption and far-IR spectra of the compounds are reported. Compounds 2–7 melt congruently in the 540–773°C region, whereas 1 melts incongruently. © 1998 Academic Press

1. INTRODUCTION

Recently, there has been a resurgence of polychalcophosphate chemistry through the use of fluxes and this has led to many new ternary and quaternary chalcophosphate compounds (1). The $A_x[P_yQ_z]$ (Q = S, Se) fluxes provide various $[P_yQ_z]^{n-}$ anions which, in the presence of metal ions, coordinate to give interesting new solid state or molecular materials. Many unusual compounds containing main-group metals (2), transition metals (3), lanthanides and actinides (2e, 2f, 4) have been reported. We have now examined the reactivity of Group 10 and Group 12 metals in these melts and have already reported on the discrete molecular cluster compounds $[M_4(Se_2)_2(PSe_4)_4]^{8-}$ (M = Cd, Hg) (3d) as well as on the palladium compounds $A_4Pd(PQ_4)_2$ (A = K, Cs; Q = S, Se), $Cs_{10}Pd(PSe_4)_4$, $KPdPS_4$, and $K_2PdP_2S_6$ (3g). Herein, we report the synthesis, structure, and optical and thermal properties of the one-dimensional selenodiphosphates $Cs_2PdP_2Se_6$ (**1**) (3g) $K_2ZnP_2Se_6$ (**2**), $K_2CdP_2Se_6$ (**3**), $Rb_2CdP_2Se_6$ (**4**), $Cs_2CdP_2Se_6$ (**5**), $K_2HgP_2Se_6$ (**6**), and $Rb_2HgP_2Se_6$ (**7**). Single-crystal X-ray diffraction analysis was performed for compounds **1**, **4**, and **6**, representing the three different structure types. Compounds **1–7** contain the ethane-like $[P_2Se_6]^{4-}$ unit in different coordination modes.

2. EXPERIMENTAL

2.1. Reagents

The reagents mentioned in this study were used as obtained unless noted otherwise.

2.2. Syntheses

A_2Q (A = K, Rb, Cs; Q = S, Se) were prepared by reacting stoichiometric amounts of the elements in liquid ammonia as described elsewhere (2).

Preparation of $Cs_2PdP_2Se_6$ (**1**). The preparation of this compound has been described elsewhere (3g).

Preparation of $K_2ZnP_2Se_6$ (**2**). A mixture of Zn (0.25 mmol), P_2Se_5 (0.75 mmol), K_2Se (1.00 mmol), and Se (2.50 mmol) was sealed under vacuum in a Pyrex tube and heated to 500°C for 4 days followed by cooling to 150°C at 2°C h^{-1}. Most of the excess $K_xP_ySe_x$ flux was removed with degassed DMF. The product was then washed with ~2ml of tri-*n*-butyl phosphine to remove elemental Se. Further washing with anhydrous ether revealed an intimate mixture of yellow microcrystals (~70%) and residual flux in the form of gray powder (~30%). The crystals were air- and

[1]To whom correspondence should be addressed. E-mail: kanatzid@argus.cem.msu.edu.

0022-4596/98 $25.00

water-stable. Microprobe analysis with a scanning electron microscope (SEM) performed on a large number of single crystals gave an average composition of $K_{2.1}ZnP_{2.1}Se_{5.9}$.

Preparation of $K_2CdP_2Se_6$ (**3**). A mixture of Cd (0.25 mmol), P_2Se_5 (0.75 mmol), K_2Se (1.00 mmol), and Se (2.50 mmol) was prepared as for **2** and heated with the same heating profile. Isolation as in **2** revealed dark yellow, rodlike crystals that were air- and water-stable (Yield $\sim$65% based on Cd). Microprobe analysis gave an average composition of $K_{1.9}CdP_{2.2}Se_{6.0}$.

Preparation of $Rb_2CdP_2Se_6$ (**4**). A mixture of Cd (0.25 mmol), P_2Se_5 (0.75 mmol), Rb_2Se (1.00 mmol), and Se (2.50 mmol) was prepared as for **2** and heated with the same heating profile. Isolation as in **2** revealed dark yellow, rodlike crystals (1–2 mm) that were air- and water-stable (yield $\sim$75% based on Cd). Microprobe analysis gave an average composition of $Rb_{2.2}CdP_{2.0}Se_{6.1}$.

Preparation of $Cs_2CdP_2Se_6$ (**5**). A mixture of Cd (0.25 mmol), P_2Se_5 (0.75 mmol), Cs_2Se (0.50 mmol), and Se (2.50 mmol) was prepared as for **2** and heated with the same heating profile. Isolation as in **2** revealed yellow, rodlike crystals that were air- and water-stable (Yield ·69% based on Cd). Microprobe analysis gave an average composition of $Cs_{2.0}CdP_{2.1}Se_{5.9}$.

Preparation of $K_2HgP_2Se_6$ (**6**). A mixture of HgSe (0.25 mmol), P_2Se_5 (0.75 mmol), K_2Se (1.00 mmol), and Se (2.50 mmol) was prepared as for **2** and heated with the same heating profile. Isolation as in **2** revealed dark yellow, rodlike crystals that were air- and water-stable (yield $\sim$79% based on Hg). Microprobe analysis gave an average composition of $K_{1.9}HgP_{2.1}Se_{5.8}$.

Preparation of $Rb_2HgP_2Se_6$ (**7**). A mixture of HgSe (0.25 mmol), P_2Se_5 (0.75 mmol), Rb_2Se (0.50 mmol), and Se (2.50 mmol) was prepared as for **2** and heated with the same heating profile. Isolation as in **2** revealed dark yellow, rodlike crystals that were air- and water-stable (yield $\sim$74% based on Hg). Microprobe analysis gave an average composition of $Rb_{1.9}HgP_{1.8}Se_{6.0}$.

2.3. Physical Measurements

Powder X-ray diffraction. Analyses were performed using a calibrated Rigaku-Denki RW400F2 (Rotaflex) rotating-anode powder diffractometer controlled by an IBM computer (45 kV/100 mA, 1°/min scan rate, Ni-filtered Cu radiation). Samples were ground to a fine powder and mounted by spreading the sample onto a special etched-glass holder. Powder patterns were calculated with the CERIUS molecular modeling program (Molecular Simulations Inc., St. John's Innovation Centre, Cambridge, England). Calculated and observed XRD patterns are deposited with the supplementary material.[2]

Infrared spectroscopy. Infrared spectra, in the far-IR region (600–50 cm^{-1}), were recorded on a computer-controlled Nicolet 750 Magna-IR Series II spectrophotometer equipped with a TGS/PE detector and a silicon beam splitter spectrophotometer in 4-cm^{-1} resolution. The samples were ground with dry CsI into a fine powder and pressed into translucent pellets.

Solid state UV–Vis–near-IR spectroscopy. Optical diffuse reflectance measurements were performed at room temperature using a Shimadzu UV-3101PC double-beam, double-monochromator spectrophotometer. The instrument is equipped with an integrating sphere and controlled by a personal computer. $BaSO_4$ was used as a 100% reflectance standard for all materials. Samples were prepared by grinding them to a fine powder and spreading them on a compacted surface of the powdered standard material, preloaded into a sample holder. The reflectance versus wavelength data generated can be used to estimate a material's band gap by converting reflectance to absorption data as described earlier (5).

Single-crystal optical transmission. Room temperature single-crystal optical transmission spectra were obtained on a Hitachi U-6000 microscopic FT spectrophotometer mounted on an Olympus BH2-UMA metallurgical microscope over the range 380–900 nm. Crystals lying on a glass slide were positioned over the light source and the transmitted light was detected from above.

Differential thermal analysis (DTA). DTA experiments were performed as described elsewhere (2). The residue of the DTA experiment was examined by X-ray powder diffraction. To evaluate congruent melting, we compared the X-ray powder diffraction patterns before and after the DTA experiments as well as monitored the stability/reproducibility of the DTA diagrams upon cycling the above conditions at least two times.

Semiquantitative microprobe analyses. The analyses were performed using a JEOL JSM-6400V scanning electron microscope (SEM) equipped with a TN 5500 EDS detector. Data acquisition was performed with an accelerating voltage of 20 kV and a 30-s accumulation time.

[2]See NAPS document No. 000000 for 00 pages of supplementary material. This is — is not — a multiarticle document. Order from NAPS c/o Microfiche Publications, P.O. Box 3513, Grand Central Station, New York, NY 10163–3513. Remit in advance in U.S. funds only $7.75 for photocopies or $5.00 for microfiche. There is a $15.00 invoicing charge on all orders filled before payment. Outside U.S. and Canada add postage of $4.50 for the first 20 pages and $1.00 for each 10 pages of material thereafter, or $1.75 for the first microfiche and $.50 for each microfiche thereafter.

Single-crystal X-ray crystallography. Intensity data for **4** and **6** were collected using a Rigaku AFC6S four-circle automated diffractometer equipped with a graphite crystal monochromator. An ω–2θ scan mode was used. Crystal stability was monitored with three standard reflections whose intensities were checked every 150 reflections. No crystal decay was detected in any of the compounds. A Siemens SMART Platform CCD diffractometer was used to collect a hemisphere of data for **1** using 35 s frames (detector-to-crystal distance was 5 cm). The space groups were determined from systematic absences and intensity statistics. The detailed structure of **1** has been reported elsewhere (3g). For **4** and **6** an empirical absorption correction based on ψ scans was applied to all data during initial stages of refinement. An empirical DIFABS correction was applied to **4** and **6** after full isotropic refinement as recommended (6b). A full anisotropic refinement was then performed. The structures were solved by direct methods using SHELXS-86 software (7a) (for all compounds) and refined with full-matrix least-squares techniques available in the TEXSAN software package (7b). Crystallographic information for the compounds is given in Table 1. The coordinates of all atoms, equivalent isotropic temperature factors, and their estimated standard deviations are given in Tables 2 and 3.

TABLE 1
Crystallographic Data for $Rb_2CdP_2Se_6$ and $K_2HgP_2Se_6$

Formula	$Rb_2CdP_2Se_6$ (**4**)	$K_2HgP_2Se_6$ (**6**)
FW	819.05	814.49
a (Å)	6.640(1)	13.031(2)
b (Å)	12.729(2)	7.308(2)
c (Å)	7.778(1)	14.167(2)
β (deg)	98.24(1)	110.63(1)
Z; V (Å^3)	2; 650.6(2)	4; 1262.6(4)
λ (Mo$K\alpha$) (Å)	0.71069	0.71069
Space group	$P2_1/n$ (No. 14)	$P2_1/c$ (No. 14)
D_{calc} (g/cm^3)	4.180	4.285
μ (cm^{-1})	257.18	301.77
$2\theta_{max}$ (deg)	50	55
Temperature (°C)	26	23
Final R/R_w[a] (%)	3.7/4.9	5.6/7.1
Octants collected	$h, k, \pm l$	$h, k, \pm l$
Data measured	1307	3233
Unique data/R_{int}	1201/0.103	3096/0.058
Data $F_o^2 > 3\sigma(F_o^2)$	583	2224
Number of variables	53	100
Absorption ratio (min/max)	0.648	0.382
Crystal dimensions (mm)	$0.70 \times 0.28 \times 0.22$	$0.56 \times 0.32 \times 0.10$

[a] $R = \sum(|F_o| - |F_c|)/\sum|F_o|$, $R_w = \{\sum_w(|F_o| - |F_c|)^2/\sum_w|F_o|^2\}^{1/2}$.

TABLE 2
Positional Parameters and B_{eq} for $Rb_2CdP_2Se_6$

Atom	x	y	z	B_{eq}[a] (Å)
Cd	$\frac{1}{2}$	0	$\frac{1}{2}$	2.48(7)
Rb	0.2579(3)	0.1784(1)	− 0.0211(2)	3.20(7)
Se(1)	0.2105(2)	0.1785(1)	0.4543(2)	2.16(7)
Se(2)	0.1916(2)	− 0.0701(1)	0.2364(2)	1.87(6)
Se(3)	0.2176(2)	0.4256(1)	0.7467(2)	2.03(7)
P	0.0237(5)	0.0404(3)	0.3753(5)	1.1(1)

[a] $B_{eq} = (4/3)[a^2B(1,1) + b^2B(2,2) + c^2B(3,3) + ab(\cos\gamma)B(1,2) + ac(\cos\beta)\,B(1,3) + bc(\cos\alpha)B(2,3)]$.

3. RESULTS AND DISCUSSION

3.1. Description of Structures

Compounds **1**–**7** belong to the $A_2MP_2Q_6$ (A = K, Rb, Cs; M = Mn, Fe; Q = S, Se) family of compounds that was observed during studies with the transition metals (3a, 8). In addition to this structure type, in this work, we encountered a new structure type in $K_2HgP_2Se_6$, which is related to that of $Cs_2PdP_2Se_6$ (3g).

$Cs_2PdP_2Se_6$, whose structure has been described in detail earlier (3g), has the one-dimensional structure shown in Fig. 1A. The structure features the $[P_2Se_6]^{4-}$ group, which acts as a bridging multidentate ligand for two square-planar Pd^{2+} atoms, utilizing four out of the six possible coordination sites. The chains propagate in the [001] direction. The phosphorus positions were found to be disordered inside the essentially fixed Se octahedral pocket, adopting four different orientations [P(1)–P(1), P(2)–P(2), P(3)–P(4) × 2]; see Fig. 1B. Each P–P pair is oriented in such a way that (a) it is perpendicular to opposite faces of the octahedron and (b) the center of the Se octahedron is located in the middle of the P–P bonds. This disorder arises from the fact that there

TABLE 3
Positional Parameters and B_{eq} for for $K_2HgP_2Se_6$

Atom	x	y	z	B_{eq}[a] (Å^2)
Hg	0.74271(5)	0.10675(9)	0.97753(6)	2.14(3)
Se(1)	0.5991(1)	0.3313(2)	1.0002(1)	1.51(5)
Se(2)	0.6195(2)	0.0114(2)	1.2039(1)	2.60(7)
Se(3)	0.6412(1)	− 0.2206(2)	0.9461(1)	1.74(6)
Se(4)	0.9084(1)	0.0112(3)	1.1473(1)	2.24(6)
Se(5)	0.8421(1)	0.1884(2)	0.8511(1)	1.87(6)
Se(6)	0.8865(1)	− 0.3021(2)	0.8955(2)	2.38(7)
K(1)	0.6013(4)	− 0.0524(7)	0.7152(3)	3.9(2)
K(2)	1.1017(4)	0.0376(7)	1.3784(4)	4.1(2)
P(1)	0.5192(3)	0.1120(5)	1.0592(3)	1.3(1)
P(2)	1.0389(3)	0.0360(5)	1.0829(3)	1.4(1)

[a] $B_{eq} = (4/3)[a^2B(1,1) + b^2B(2,2) + c^2B(3,3) + ab(\cos\gamma)B(1,2) + ac(\cos\beta)B(1,3) + bc(\cos\alpha)B(2,3)$.

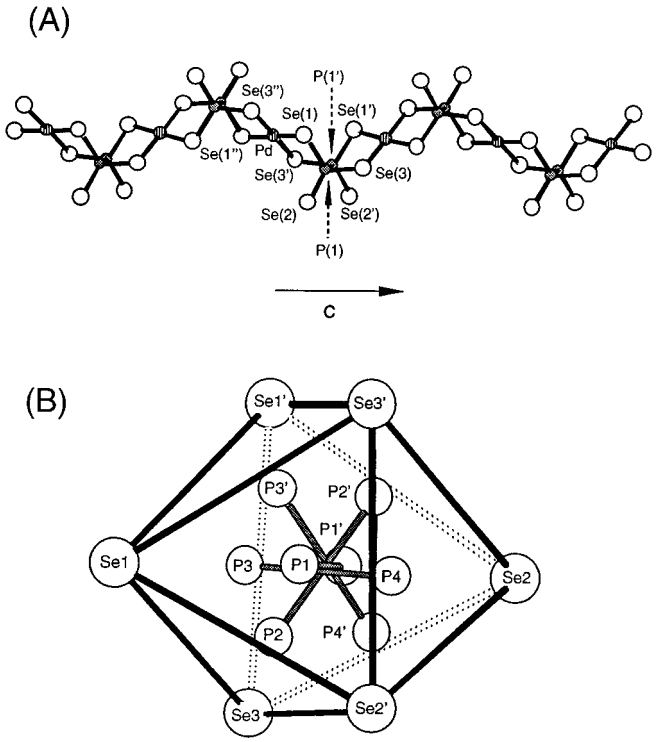

FIG. 1. (A) An isolated $[PdP_2Se_6]_n^{2n-}$ chain with labeling. (B) Disorder of the P atoms in the $[P_2Se_6]^{4-}$ group. Bonds between P and Se atoms are omitted for clarity.

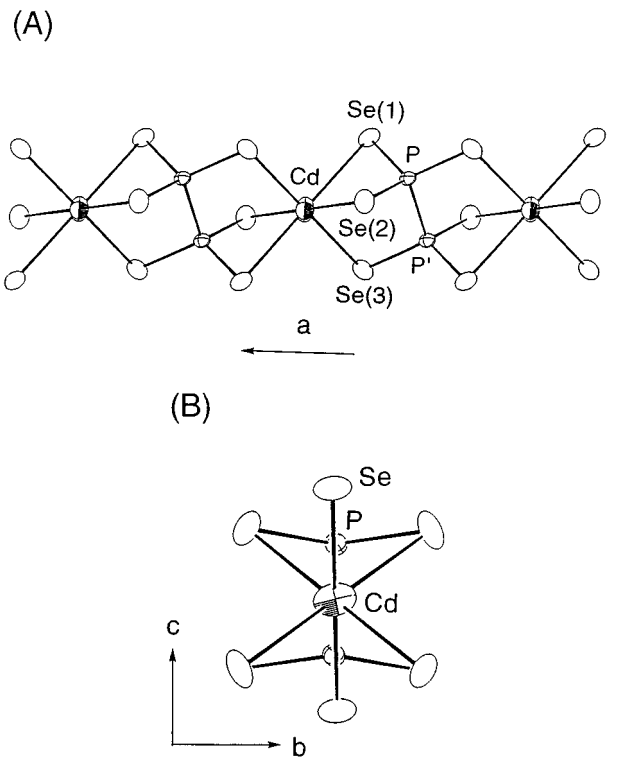

FIG. 2. (A) ORTEP representation and labeling of a single $[CdP_2Se_6]^{2n-}$ chain (70% probability). (B) Projection of the chain on the *b*–*c* plane.

is no energetically favored orientation for the P–P pairs, since the Se octahedron is almost ideal. The staggered conformation of the ethane-like $[P_2Se_6]^{4-}$ causes the neighboring square-planar Pd^{2+} atoms to rotate their planes will respect to each other. Nevertheless, the Pd atoms are aligned parallel to the *c* axis. The Pd–Se distances average at 2.466(7) Å and they are in good agreement with those found in other polyselenides with square-planar Pd^{2+}, e.g., $Cs_4Pd(PSe_4)_2$ (3g), $Cs_{10}Pd(PSe_4)_4$ (3g), and $K_2[PdSe_{10}]$ (9).

Compounds **2**–**5** have one-dimensional chains propagating down the [100] direction, as shown in Fig. 2A. They also feature the $[P_2Se_6]^{4-}$ group, which coordinates to the octahedral M^{2+} atoms. Zinc and cadmium adopt octahedral coordination, which is rare for these two elements (10), although octahedral coordination is observed in the ternary $M_2P_2S_6$ (M = Zn, Cd) (11, 12) Compounds **2**–**5** are isostructural with $A_2MP_2Se_6$ (A = K, Rb; M = Mn, Fe) (3a), which is closely related to the TiI_3 type (Ti_2I_6 by doubling the formula). The $[MP_2Se_6]_n^{2n-}$ anion can be viewed as an ordered substitution of the Ti atoms by M and P–P pairs and of the I atoms by Se. Both the M^{2+} ion and the P–P pairs reside in Se octahedra that share opposite faces. The M octahedra are fully eclipsed when viewed along the chain axis; see Fig. 2B. For **4** the Cd–Se distances average at 2.85(9) Å, with the axial Se(1) displaying the longer distances [2.965(2) Å]. The phosphorus–phosphorus distance is 2.257(7) Å. The $[CdP_2Se_6]_n^{2n-}$ chains are separated by six-coordinate Rb^+ ions [range of Rb–Se distances, 3.489(2)–3.756(3) Å; average 3.629 Å]. Selected bond distances and angles for **4** are given in Table 4.

The Hg compounds **6** and **7** have a one-dimensional structure, which is shown in Fig. 3A. The structure contains the $[P_2Se_6]^{4-}$ group, which is bridging tetradentate as in **1**.

TABLE 4
Selected Distances (Å) and Angles (Deg) for $Rb_2CdP_2Se_6$

Cd–Se(1)	2.965(2)	Se(1)–Cd–Se(2)	76.41(4)
Cd–Se(2)	2.827(2)	Se(1)–Cd–Se(3)	87.25(4)
Cd–Se(3)	2.772(2)	Se(2)–Cd–Se(3)	90.60(4)
P–Se(1)	2.188(4)	Cd–Se(1)–P	75.5(1)
P–Se(2)	2.176(4)	Cd–Se(2)–P	78.8(1)
P–Se(3)	2.176(4)	Cd–Se(3)–P	98.8(1)
P–P	2.257(7)	Se(1)–P–Se(2)	110.4(2)
		Se(1)–P–Se(3)	115.1(2)
		Se(2)–P–Se(3)	114.3(2)
		Se(1)–P–P′	105.5(2)

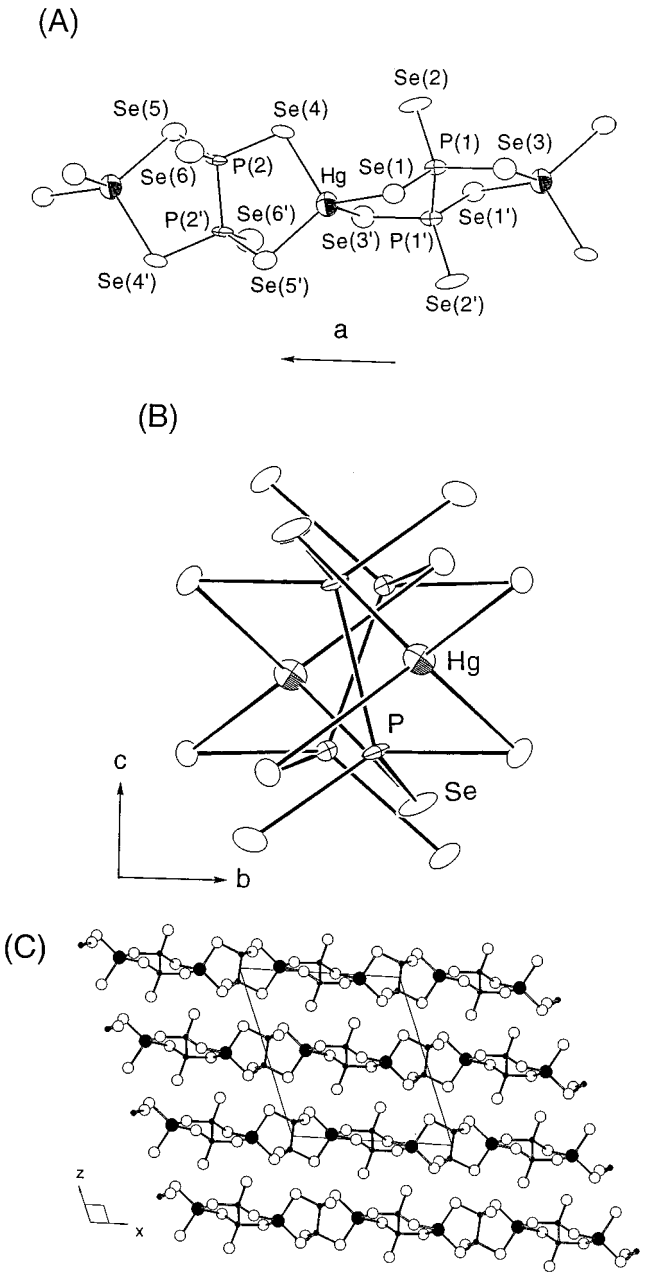

FIG. 3. (A) ORTEP representation and labeling of a single $[HgP_2Se_6]^{2n-}$ chain (80% probability). (B) Projection of the chain on the *b*–*c* plane. (C) Unit cell of $K_2HgP_2Se_6$. K atoms are omitted.

The major difference between this structure and the structure of **2**–**5** is that the larger Hg^{2+} is tetrahedral. To accommodate that, the $[P_2Se_6]^{4-}$ adjusts both its denticity and its arrangement in the chain. Consequently, the neighboring P–P pairs are tilted with respect to each other and are not parallel as in **2**–**5**; see Fig. 3B. The related compound $Hg_2P_2Se_6$ (13) also features the $[P_2Se_6]^{4-}$ ligand and tetrahedral Hg^{2+}. It can be regarded as the parent compound of **6** and **7** since one can envision "dismantling" the 2-D network of $Hg_2P_2Se_6$ by substituting one Hg^{2+} for two A^+ ions, to obtain the 1-D chains of $A_2HgP_2Se_6$; see Eq. [1].

$$\underset{\text{(2-D)}}{Hg_2P_2Se_6} \xrightarrow[+2A^+]{-Hg^{2+}} \underset{\text{(1-D)}}{A_2HgP_2Se_6} \qquad [1]$$

A single $Hg_2P_2Se_6$ layer is shown in Fig. 4A. Removal of half of the Hg^{2+} cations yields the $[HgP_2Se_6]^{2-}$ layer as shown in Fig. 4B. To maintain electroneutrality, two alkali metal ions must be introduced. This metal-deficient structure may very well be stable with the proper counterion, but the lack of available space for a low-energy packing arrangement for the alkali metal atoms within the layer causes a structural change to a one-dimensional structure. This generates more space for efficient packing of the alkali ions. This effect can be understood in terms of the counterion effect, which has been discussed earlier (14).

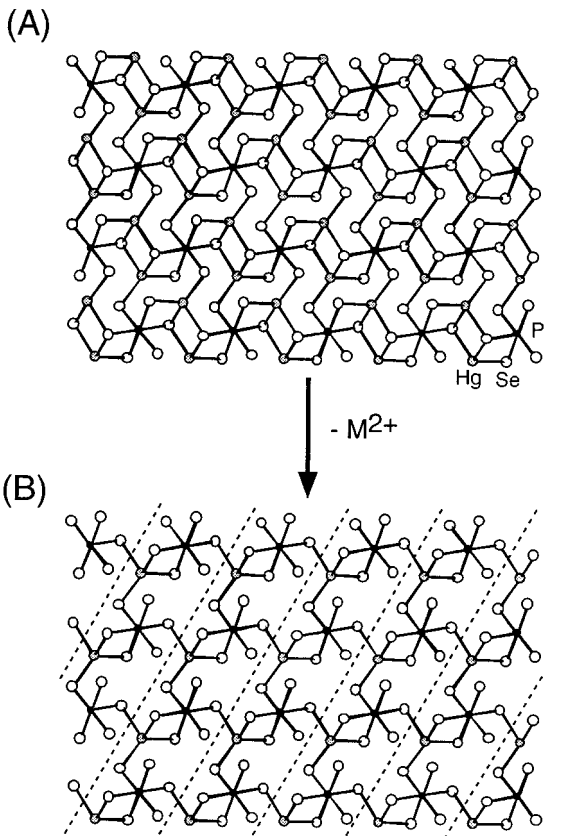

FIG. 4. (A) A single $Hg_2P_2Se_6$ layer. (B) Removal of half of the Hg^{2+} ions, resulting in a hypothetical $[HgP_2Se_6]^{2-}$ layer. Dashed lines highlight the possibility of chain formation by breaking the corresponding Hg–Se bonds. In this view the projection of the $[P_2Se_6]^{4-}$ units is down the P–P bond, which gives the illusionary appearance of an octahedron.

For **6** the Hg–Se distances average at 2.65(5) Å and they compare very well with those of $Hg_2P_2Se_6$. The phosphorus–phosphorus distances average at 2.268(8) Å. The $[HgP_2Se_6]_n^{2n-}$ chains are close packed in a pseudohexagonal arrangement and are separated by alkali cations. Both of the alkali cations, K(1) and K(2), are rather oddly coordinated by Se atoms [range of K(1)–Se distances, 3.352(5)–3.521(5) Å, average 3.417 Å; range of K(2)–Se distances, 3.360(6)–3.478(6) Å, average 3.393 Å]. The irregular sites for K(1) and K(2) are shown in Fig. 5. Selected bond distances and angles for **6** are given in Table 5.

Because a series of analogous compounds has been generated, it is useful at this point to draw some conclusions about the structural influence of the M^{2+} size on the $[P_2Se_6]^{4-}$ group. In $A_2MP_2Se_6$ (M = Mn, Fe, Pd, Cd, Hg), a comparison of the M^{2+} ionic radius (15) with the P–P distance in the $[P_2Se_6]^{4-}$ group reveals a positive correlation between the two, where the larger the metal, the longer the P–P bond; see Fig. 6. This suggests that $[P_2Se_6]^{4-}$ can be viewed as a dimer of two PSe_3 groups connected via a relatively weak P–P bond. The latter can be easily stretched or shrunk, varying the Se–Se "bite" size, so it can accommodate different sizes of metal ions. A similar trend is observed for the $[P_2S_6]^{4-}$ group in the MPS_3 phases (16).

TABLE 5
Selected Distances (Å) and Angles (deg) for $K_2HgP_2Se_6$

Hg–Se(1)	2.592(2)	Se(1)–Hg–Se(3)	104.40(5)
Hg–Se(3)	2.694(2)	Se(1)–Hg–Se(4)	116.08(6)
Hg–Se(4)	2.697(2)	Se(1)–Hg–Se(5)	119.49(6)
Hg–Se(5)	2.622(2)	Se(3)–Hg–Se(4)	96.31(6)
		Se(3)–Hg–Se(5)	114.91(6)
P(1)–Se(1)	2.228(4)		
P(1)–Se(2)	2.137(5)	Hg–Se(1)–P(1)	92.5(1)
P(1)–Se(3)	2.212(4)	Hg–Se(3)–P(1)	95.2(1)
P(2)–Se(4)	2.202(4)	Hg–Se(4)–P(2)	95.9(1)
P(2)–Se(5)	2.223(4)	Hg–Se(5)–P(2)	89.1(1)
P(2)–Se(6)	2.148(4)		
		Se(1)–P(1)–Se(2)	113.5(2)
P(1)–P(1)	2.269(8)	Se(1)–P(1)–Se(3)	106.8(2)
P(2)–P(2)	2.268(8)	Se(2)–P(1)–Se(3)	114.0(2)
		Se(4)–P(2)–Se(5)	106.9(2)
		Se(4)–P(2)–Se(6)	113.1(2)
		Se(5)–P(2)–Se(6)	113.2(2)
		Se(1)–P(1)–P(1′)	104.6(3)
		Se(3)–P(1′)–P(1)	105.9(2)
		Se(4)–P(2)–P(2′)	106.3(2)
		Se(5)–P(2′)–P(2)	104.8(2)

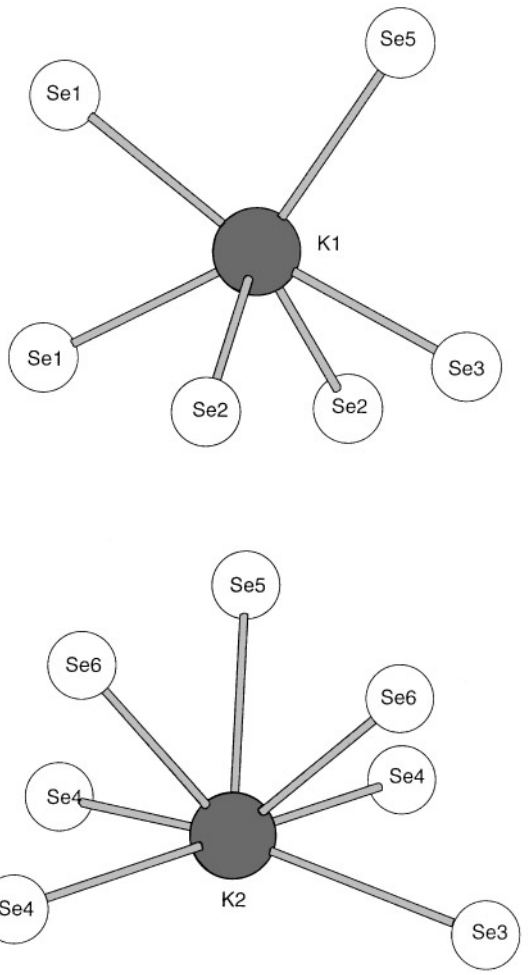

FIG. 5. Immediate environment of the potassium atoms in $K_2HgP_2Se_6$ drawn out to 3.9-Å radius.

3.2. Synthesis, Spectroscopy, and Thermal Analysis

The new compounds were obtained by the oxidative dissolution of the appropriate metal in a polyselenophosphate

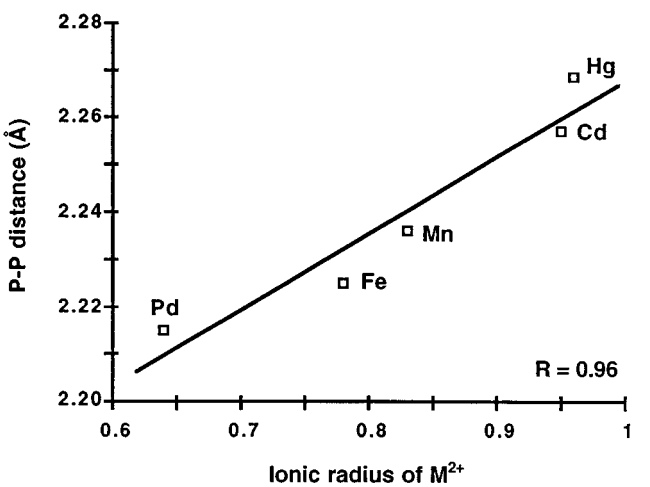

FIG. 6. Diagram of the P–P distance vs M^{2+} ionic radius in $A_2MP_2Se_6$.

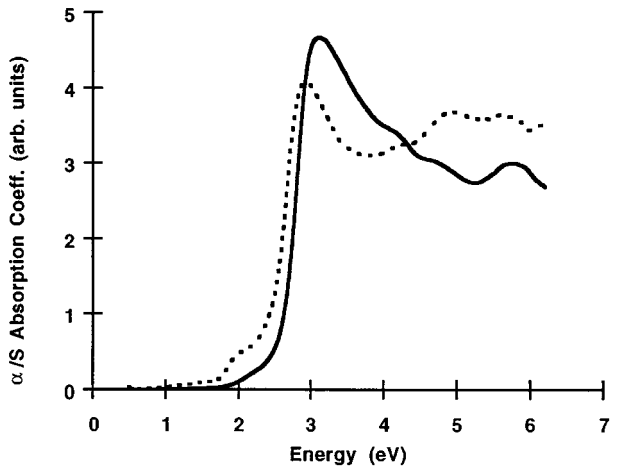

FIG. 7. Optical absorption spectra of $Rb_2CdP_2Se_6$ (solid line) and of $Rb_2HgP_2Se_6$ (dotted line).

flux. The metal cations are coordinated *in situ* by the highly charged $[P_2Se_6]^{4-}$ ligands present in the flux. Even though all compounds have the same $A_2MP_2Se_6$ formula, we observe three different, but closely related, structure types which result from the different coordination requirements and/or preferences of the metal ions. The relatively Se-rich conditions used in the syntheses yielded compounds with the $[P_2Se_6]^{4-}$ ligand, which contains P^{4+}. If higher basicity conditions are employed (by increasing the A_2Se content), compounds with P^{5+} atoms, i.e., with the $[PSe_4]^{3-}$ ligand, are formed (3d–g). This is now a general theme in this chemistry (2f, 3b, 4b).

All compounds are wide-gap semiconductors as determined by optical absorption spectroscopy; see Fig. 7. The band gaps, E_g, are given in Table 6. Data for **2** are not reliable because of the presence of impurities.

The transparent well-formed crystals of **4** were suitable for single-crystal optical transmission measurements. This served two purposes: first, to evaluate the nature of the band gap in the $A_2CdP_2Se_6$ phases and second, to provide an estimation of the agreement between the E_g values obtained from powder (reflectance) and single-crystal (transmission) data. The spectrum from a single crystal of **4**, converted to absorption data, is shown in Fig. 8A. The absorption edge is

TABLE 6
Optical Band Gaps and Melting Point Data[a]

Formula	E_g (eV)	MP (°C)
$Cs_2PdP_2Se_6$	1.60	615[i]
$K_2CdP_2Se_6$	2.58	640
$Rb_2CdP_2Se_6$	2.58 (2.66)[t]	720
$Cs_2CdP_2Se_6$	2.63	773
$K_2HgP_2Se_6$	2.25	541
$Rb_2HgP_2Se_6$	2.32	578

[a] i, incongruent melting; t, from single-crystal transmission data.

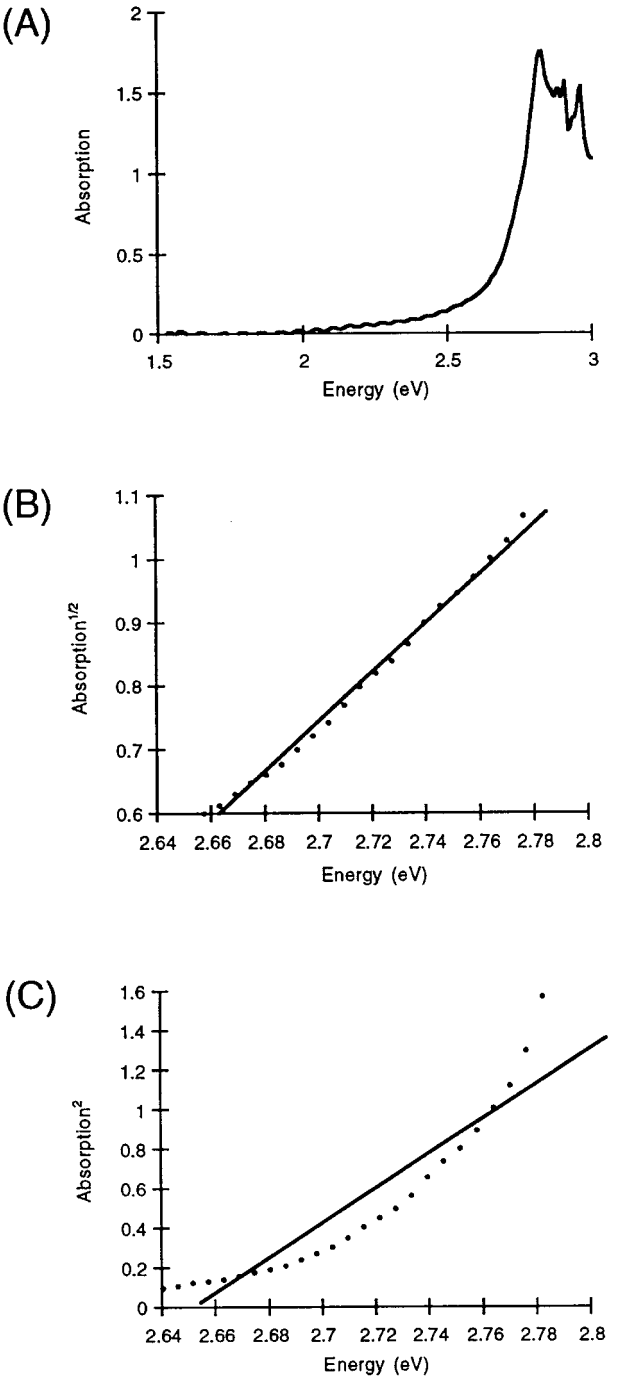

FIG. 8. (A) Single-crystal optical transmission spectrum of $Rb_2CdP_2Se_6$ converted to absorption data. (B) The region close to the absorption edge is plotted for absorption$^{1/2}$ vs energy. (C) The same region is plotted for absorption^2 vs energy.

much steeper than that from the diffuse reflectance spectrum but gives a very similar band gap ($E_g = 2.66$ eV). The absorption$^{1/2}$ vs energy plot (Fig. 8B) is very nearly linear ($R = 0.99$), while the plot of absorption^2 vs energy (Fig. 8C) deviates significantly from linearity ($R = 0.93$). This suggests (17) that **4** has an indirect band gap.

The far-IR spectra of **1** display strong absorptions at ca. 490, 442, and 306 cm^{-1}. Compounds **2**–**7** have nearly identical spectra, displaying strong absorptions at ca. 475, 465, and 304 cm^{-1}. The vibrations at ca. 490, 475, 465, and 442 cm^{-1} can be assigned to PSe_3 stretching modes and the vibrations at ca. 304 and 306 cm^{-1} to the out-of-phase translational PSe_3 mode (3a). All compounds possess weak absorptions below 200 cm^{-1}, which probably are due to M–Se vibrations (3).

Differential thermal analysis (DTA) measurements followed by XRD analysis of the residues suggest that **2**–**7** melt congruently (see Table 6), whereas **1** melts incongruently, yielding binary Pd/Se phases and amorphous $Cs_xP_ySe_z$.

4. CONCLUDING REMARKS

The synthesis of new members of the $A_2MP_2Se_6$ family has been accomplished with the use of polyselenophosphate $A_x[P_ySe_z]$ fluxes. This general class seems to be very stable, and so far, compounds with this formula have been synthesized from Groups 7, 8, 10, and 11. Given that some sulfide members also exist (e.g., $K_2MP_2S_6$; M = Mn, Fe) (8), the size of the $A_2MP_2Q_6$ family could approach that of the ternary $M_2P_2Q_6$. The observed P–P bond elasticity according to metal ion size provides additional flexibility for these structures to form. It would be interesting to see if members of this family with appropriate alkali ions are soluble in polar solvents (18).

ACKNOWLEDGMENTS

Financial support from the National Science Foundation (Grant DMR-9527347) is gratefully acknowledged. M.G.K. is a Camille and Henry Dreyfus Teacher–Scholar (1993–1998). This work made use of the SEM facilities of the Center for Electron Optics at Michigan State University.

REFERENCES

1. M. G. Kanatzidis, *Curr. Opin. Solid State Mater. Sci.* **2,** 139 (1997).
2. (a) T. J. McCarthy and M. G. Kanatzidis, *Chem. Mater.* **5,** 1061 (1993); (b) T. J. McCarthy and M. G. Kanatzidis, *J. Chem. Soc., Chem. Commun.* 1089 (1994); (c) T. J. McCarthy, T. Hogan, C. R. Kannewurf, and M. G. Kanatzidis, *Chem. Mater.* **6,** 1072 (1994); (d) T. J. McCarthy and M. G. Kanatzidis, *J. Alloys Compd.* **236,** 70 (1996); (e) K. Chondroudis and M. G. Kanatzidis, Materials Research Society, Fall 1996 Meeting, Boston, MA; (f) K. Chondroudis, T. J. McCarthy, and M. G. Kanatzidis, *Inorg. Chem.* **35,** 840 (1996); (g) K. Chondroudis and M. G. Kanatzidis, *J. Chem. Soc., Chem. Commun.* 1371 (1996).
3. (a) T. J. McCarthy and M. G. Kanatzidis, *Inorg. Chem.* **34,** 1257 (1995); (b) K. Chondroudis and M. G. Kanatzidis, *Inorg. Chem.* **34,** 5401 (1995); (c) K. Chondroudis, T. J. McCarthy, and M. G. Kanatzidis, *Inorg. Chem.* **35,** 3451 (1996); (d) K. Chondroudis and M. G. Kanatzidis, *J. Chem. Soc., Chem. Commun.* 401 (1997); (e) K. Chondroudis, M. G. Kanatzidis, *Angew. Chem.* **36,** 1324 (1997); (f) K. Chondroudis, J. A. Hanko, and M. G. Kanatzidis, *Inorg. Chem.* **36,** 2623 (1997); (g) K. Chondroudis, M. G. Kanatzidis, J. Sayettat, S. Jobic, and R. Brec, *Inorg. Chem.* **36,** 5859 (1997).
4. (a) K. Chondroudis and M. G. Kanatzidis, *C. R. Acad. Sci. Paris, Ser. B* **322,** 887 (1996); (b) K. Chondroudis and M. G. Kanatzidis, *J. Am. Chem. Soc.* **119,** 2574 (1997).
5. T. J. McCarthy, S.-P. Ngeyi, J.-H. Liao, D. DeGroot, T. Hogan, C. R. Kannewurf, and M. G. Kanatzidis, *Chem. Mater.* **5,** 331 (1993).
6. (a) R. H. Blessing, *Acta Crystallogr., Sect. A* **51,** 33 (1995); (b) N. Walker and D. Stuart, *Acta Crystallogr., Sect A* **39,** 158 (1983).
7. (a) G. M. Sheldrick, "Crystallographic Computing 3" (G. M. Sheldrick, C. Kruger, and R. Doddard, Eds.), p. 175. Oxford University Press, Oxford, England, 1985; (b) G. J. Gilmore, *Appl. Crystallogr.* **17,** 42 (1984).
8. (a) F. Menzel, W. Brockner, W. Carrillo-Cabrera, and J. Sabmannhausen, *Z. Anorg. Allg. Chem.* **620,** 1081 (1994); (b) W. Carrillo-Cabrera, J. Sabmannhausen, H. G. Schnering, F. Menzel, and W. Brockner, *Z. Anorg. Allg. Chem.* 620, 489 (1994).
9. K.-W. Kim and M. G. Kanatzidis, *J. Am. Chem. Soc.* **114,** 4878 (1992).
10. F. A. Cotton and G. Wilkinson, "Advanced Inorganic Chemistry." J. Wiley and Sons, New York, 1988.
11. E. Prouzet, G. Ouvrard, and R. Brec, *Mater. Res. Bull.* **21,** 195 (1986).
12. G. Ouvrard, R. Brec, and J. Rouxel, *Mater. Res. Bull.* **20,** 1181 (1985).
13. M. Z. Jandali, G. Eulenberger, and H. Hahn, *Z. Anorg. Allg. Chem.* **447,** 105 (1978).
14. M. G. Kanatzidis, *Phosphorus, Sulfur, Silicon* **93**–**94,** 159 (1994).
15. The revised effective ionic radii for halides and chalcogenides by Shannon were used. For Fe^{2+} and Mn^{2+} high-spin configuration was assumed based on the magnetic measurements performed for $A_2MP_2Se_6$ (3a). R. D. Shannon, *Acta Crystallogr., Sect. A* 751 (1976).
16. R. Brec, G. Ouvrard, and J. Rouxel, *Mater. Res. Bull.* **20,** 1257 (1985).
17. J. I. Pankove, "Optical Processes in Semiconductors," pp. 34–42, Dover Publications, New York, 1971.
18. K. Chondroudis, M. G. Kanatzidis, J. Sayettat, S. Jobic, and R. Brec, work in progress.